Paper AAS 98-146

# MARS PATHFINDER ATMOSPHERIC ENTRY RECONSTRUCTION

**David A. Spencer**
**Sam W. Thurman**
**Chia-Yen Peng**
**Pieter H. Kallemeyn**

Jet Propulsion Laboratory
California Institute of Technology
Pasadena, California

**Robert C. Blanchard**
**Robert D. Braun**

NASA Langley Research Center
Hampton, Virginia

**AAS/AIAA Space Flight Mechanics Meeting**

**Monterey, California 9–11 February 1998**

**AAS Publications Office, P.O. Box 28130, San Diego, CA 92128**

AAS 98-146

# MARS PATHFINDER ATMOSPHERIC ENTRY RECONSTRUCTION

David A. Spencer*, Robert C. Blanchard#, Sam W. Thurman*,
Robert D. Braun†, Chia-Yen Peng§, Pieter H. Kallemeyn¶

The primary objective of the Mars Pathfinder mission was to demonstrate an innovative, low-cost and reliable method for placing a science payload on the surface of Mars. This paper describes the results of an effort to assess the spacecraft performance during Entry, Descent and Landing. Analysis of the raw accelerometer and altimeter flight data obtained by the Pathfinder spacecraft during atmospheric flight is provided. Results of an effort to reconstruct the spacecraft trajectory are presented. Preliminary findings of the multibody dynamics during terminal descent are described. An estimate of the Mars atmosphere profile encountered during atmospheric flight is given.

## INTRODUCTION

Five minutes after entering the Martian atmosphere, the Mars Pathfinder spacecraft impacted the surface of the Red Planet, and bounced and rolled to a stop, thus beginning a science mission that has proven to revolutionize our understanding of Mars[1]. However, the primary purpose for the Pathfinder mission was conceived to be the demonstration of a unique, low-cost method for placing science payloads on the surface of Mars. Toward this end, reconstruction of the Mars Pathfinder Entry, Descent and Landing (EDL) system performance from flight data is a critical legacy of this technology demonstration mission.

This paper presents the results of an effort to reconstruct the Pathfinder atmospheric entry trajectory, and assess the performance of the EDL system. In addition, a reconstruction of the Mars atmosphere profile encountered by the Pathfinder entry vehicle is presented.

---

* Mars Program Office, Jet Propulsion Laboratory, California Institute of Technology
# Aero- and Gas-Dynamics Division, NASA Langley Research Center
§ Mechanical Engineering Section, Jet Propulsion Laboratory, California Institute of Technology
† Space Systems & Concepts Division, NASA Langley Research Center
¶ Navigation and Flight Mechanics Section, Jet Propulsion Laboratory, California Institute of Technology

## ENTRY, DESCENT AND LANDING SEQUENCE OF EVENTS

The Pathfinder spacecraft entered Martian atmosphere directly from the Earth-to-Mars interplanetary transfer trajectory, with an inertial velocity of 7.26 km/s. The Pathfinder EDL sequence of events is shown in Figure 1. Thirty minutes prior to atmospheric entry, the cruise stage was jettisoned. The entry vehicle reached maximum stagnation point heating and peak dynamic pressure during the initial 70 s of the entry phase. At 170 s past entry, a parachute was deployed, followed by the release of the heatshield 20 s later. The lander was deployed below the backshell along a 20 m bridle. At an altitude of 1.6 km above ground level (AGL), the on-board radar altimeter acquired the ground. Altimeter data was used by the flight software to inflate an airbag system and fire a set of three solid rockets (mounted on the backshell) at an altitude of 98 m AGL. At an altitude of 22 m, the bridle was cut, and the lander fell directly to the surface, buffered at ground impact by the airbag system. Sufficient impulse remained in the solid rockets to carry the backshell and parachute to a safe distance away from the lander.

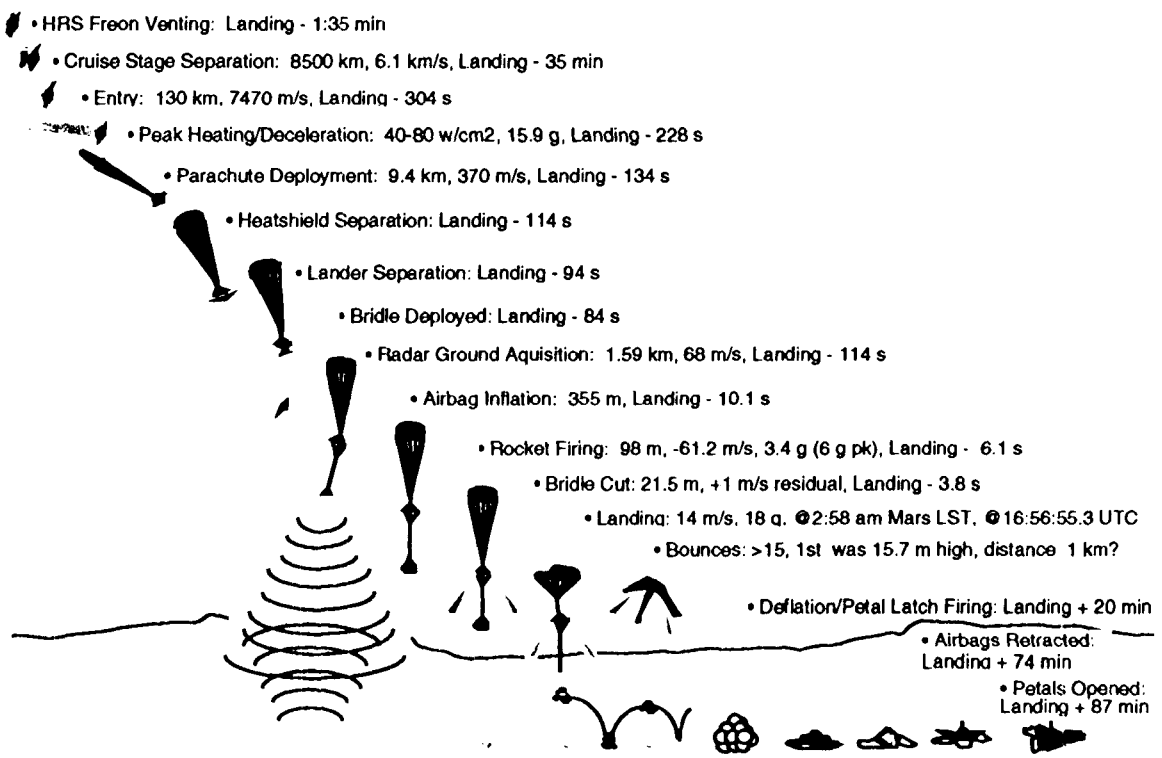


Figure 1. Mars Pathfinder EDL Sequence of Events

## EDL FLIGHT SYSTEM OVERVIEW

With the release of the cruise stage at 30 minutes prior to entry, the ability to propulsively control the spacecraft was lost. The entry vehicle was spin-stabilized with a roll rate of 2.0 rpm, and the vehicle spin axis was aligned so that the angle of attack with respect to the relative wind at the atmospheric interface (defined at a radius of 3522.2 km) would be near zero nominally. The entry vehicle mass was 585.3 kg, and the hypersonic continuum ballistic coefficient was 63.1 kg/m$^2$. The following sections briefly describe key components of the Flight System that was designed to decelerate the spacecraft from its hyperbolic entry velocity to a survivable impact velocity on the surface of Mars.

### Aeroshell

The Pathfinder aeroshell consisted of a forebody heatshield and an aftbody backshell. The aeroshell diameter was 2.65 m, and the forebody shape was a Viking-heritage 70 deg half-angle sphere-cone with a nose radius of 0.6638 m and a shoulder radius of 0.0662 m as seen in Figure 2. The forebody ablative material was SLA-561V, with a uniform thickness of 19.05 mm (0.75 in). The backshell was thermally protected with a silicon-based ablator (SIRCA) developed at Ames Research Center. The heatshield mass was 64.4 kg, and the backshell mass was 56.9 kg.

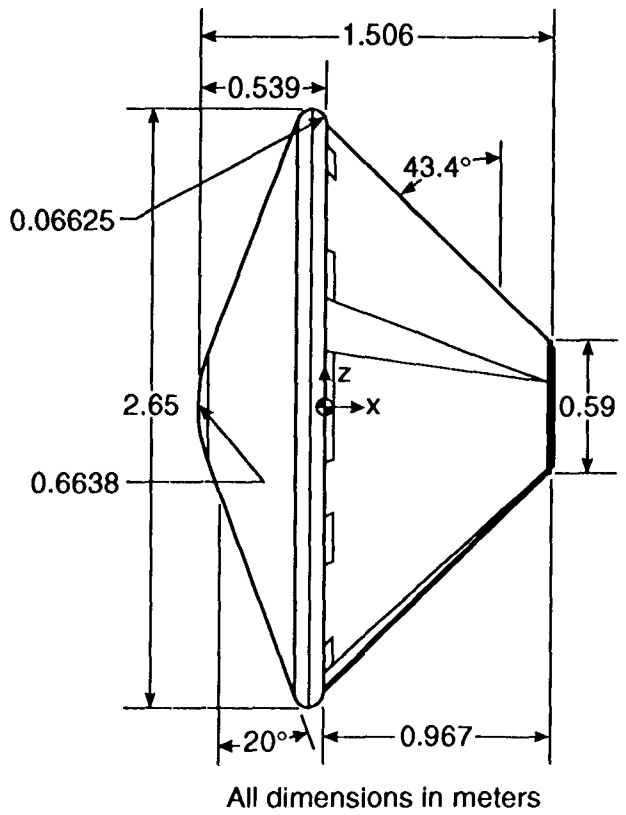


Figure 2. Pathfinder Aeroshell Dimensions

### Accelerometers

Two sets of three orthogonally-positioned Allied Signal QA-3000 accelerometer heads each provided 3-axis acceleration measurements during entry. One set of accelerometers was part of the Atmospheric Structure Investigation/Meteorology (ASI/MET) experiment. The ASI/MET accelerometers were range switched during the entry trajectory to provide increased resolution. Dynamic ranges of 16 mg, 800 mg and 40 g were used. The ASI/MET accelerometers were aligned parallel to the entry vehicle coordinate system axes. The second set of accelerometers was used as the primary input for the parachute deployment algorithm[2]. This set of engineering accelerometers was oriented such that two of the sensor heads were canted at ±45 deg to the entry vehicle Z-axis (the longitudinal axis) in the Y-Z plane, and the third accelerometer head was aligned with the X-axis. No Inertial Measurement Unit or gyros were used.

### Parachute System

The Pathfinder parachute was a modified Viking-heritage disk-gap-band design, developed by Pioneer Aerospace. The parachute canopy was made of Dacron, with Kevlar suspension lines. The Project requirement for peak dynamic pressure at parachute deployment was 703 $N/m^2$, although parachute drop tests had indicated that dynamic pressures over 800 $N/m^2$ were within the design capability. The total parachute mass was 17.5 kg.

The stowed parachute and suspension lines were packaged within an overpack, or container, which in turn was inserted into a deployment canister. Deployment was acheived through use of a mortar assembly which was initiated by an electroexplosive device.

### 20m Bridle

Following heatshield release, the lander was deployed below the backshell along a 20 m bridle. The bridle was developed at the Jet Propulsion Laboratory, and was based upon a device that is used for emergency egress of air crews from large jet aircraft when the aircraft are on the ground and stationary. The bridle consisted of a rate-limited Kevlar tether and metallic tape. A triple-bridle was attached to the single bridle at a confluence point near the backshell. The triple-bridle connected to the backshell on the brackets that support the three Rocket-Assisted Deceleration motors. The mass of the bridle was 7 kg.

### Radar Altimeter

The Honeywell HG8505DA radar altimeter was activated following heatshield release. The altimeter maximum range was specified as 5000 ft (1.52 km). The radar altimeter operated in a "first-return" mode, transmitting a series of radar pulses to the surface and clocking the time to the first received signal. Altitude data were thus provided with 1 foot resolution at a frequency of 50 Hz. The mass of the radar altimeter was 1.4 kg.

## Rocket Assisted Deceleration System

The Rocket Assisted Deceleration (RAD) system was developed by Thiokol Corporation. Three solid rocket motors, each 85 cm in length by 12.7 cm in diameter, were mounted on the backshell. The rocket motors were ignited simultaneously at a time calculated by the on-board altimeter-based RAD firing algorithm. The algorithm was designed so that the RAD system burn would bring the lander vertical velocity to zero at a nominal altitude of 15 m above the ground, with enough impulse left in the motors to carry away the backshell and parachute following the bridle cut. The motor burn duration was 2.2 s, and each rocket produced 7938 N of thrust. The total mass of the RAD system was 30.7 kg.

## Airbags

The airbag system was the key element of Pathfinder's new approach to Entry, Descent and Landing. Designed by JPL and ILC Dover, the airbag system consisted of 4 separate airbags, each with 6 lobes and a gas generator. The airbag material was Vectran, which weighed 4.8 oz/square yard. The inflated airbag system was 5.27 m wide, 4.63 m high, and 4.80 m deep. The airbag system mass was 97.7 kg. Inflation time of the airbags was 0.5 s, and the deflation/retraction time was 1.5 h.

The airbag system was rigorously tested pre-flight through drop tests at Sandia National Laboratory and the NASA Lewis Plum Brook Station chamber (see Figure 3). The system was design to withstand a vertical impact velocity of 14 m/s, and a horizontal impact velocity of 20 m/s. It was tested to land on 0.5 m high rocks without failure.

Figure 3. Airbag Drop Test at NASA Lewis Plum Brook Station Chamber

## TRAJECTORY RECONSTRUCTION

The Pathfinder entry trajectory has been reconstructed from several data sources. Radiometric tracking data taken during the interplanetary approach phase provides an estimate of the vehicle state at atmospheric entry. On-board accelerometer measurements taken during EDL provide a time-history of the entry vehicle body-fixed accelerations. Radar altimeter measurements during terminal descent are available for the final 1600 m of flight. One-way Doppler data has been constructed from the carrier signal transmitted by the spacecraft during atmospheric entry[3]. Finally, a landed position fix has been determined through landmark identification and tracking of the landed spacecraft.

### Entry State

The best solution obtained for the pre-entry trajectory utilized range and Doppler data collected from 4 February 1997, to 4 July 1997 at 15:36 UTC. Tracking data after 15:36 UTC was judged unusable since at that time the spacecraft had switched from coherent to non-coherent tracking, which reduced the precision of the data. However, this non-coherent Doppler data was later utilized in conjunction with onboard accelerometer and other spacecraft-based data.

The results of this solution were used to update and predict the conditions at the atmosphere entry point, which was defined to occur at a radial distance of 3522.2 km. This entry state serves as the initial estimate for atmospheric entry trajectory reconstruction efforts. Table 1 gives the entry state resulting from this orbit solution[4].

Table 1. Estimated Entry State from Orbit Determination

| Parameter | Orbit Determination Estimate |
|---|---|
| Epoch | 4-JUL-1997, 16:51:50.482 UTC |
| Radial Distance | 3522.2 km |
| Areocentric Latitude | 22.6303 deg |
| Longitude | 338.1691 deg |
| Inertial Flight Path Angle | -14.0610 deg |
| Inertial Velocity | 7.2642 km/s |
| Inertial Flight Path Azimuth | 253.1479 deg |

### Acceleration History

Time-ordered acceleration data showing key events during the Pathfinder entry, as measured by the ASI/MET accelerometers, are given in the series of figures labeled Figure 4 through Figure 8. These figures are presented in time segments starting at the atmospheric entry interface and extending beyond touchdown.

Figure 4 presents the initial 40 s of the entry trajectory starting at the time which corresponds to the entry interface radius of 3352.2 km. The normal acceleration (lower

plot) is the RSS of the two accelerometers normal to the axial acceleration (top plot). Namely,

$$A_n = \sqrt{A_x^2 + A_y^2} \tag{1}$$

The axial accelerometer data shows the acceleration disturbance created when the instrument detects an automatic uprange condition. This spurious spike in the data is also seen on the subsequent figures. The normal acceleration disturbance, at about 29 s, is attributed to the removal of the Kapton thermal shield which protected the probe during interplanetary cruise phase. Details of the Pathfinder spacecraft's flight through this rarefied atmospheric regime are presented in Reference 5.

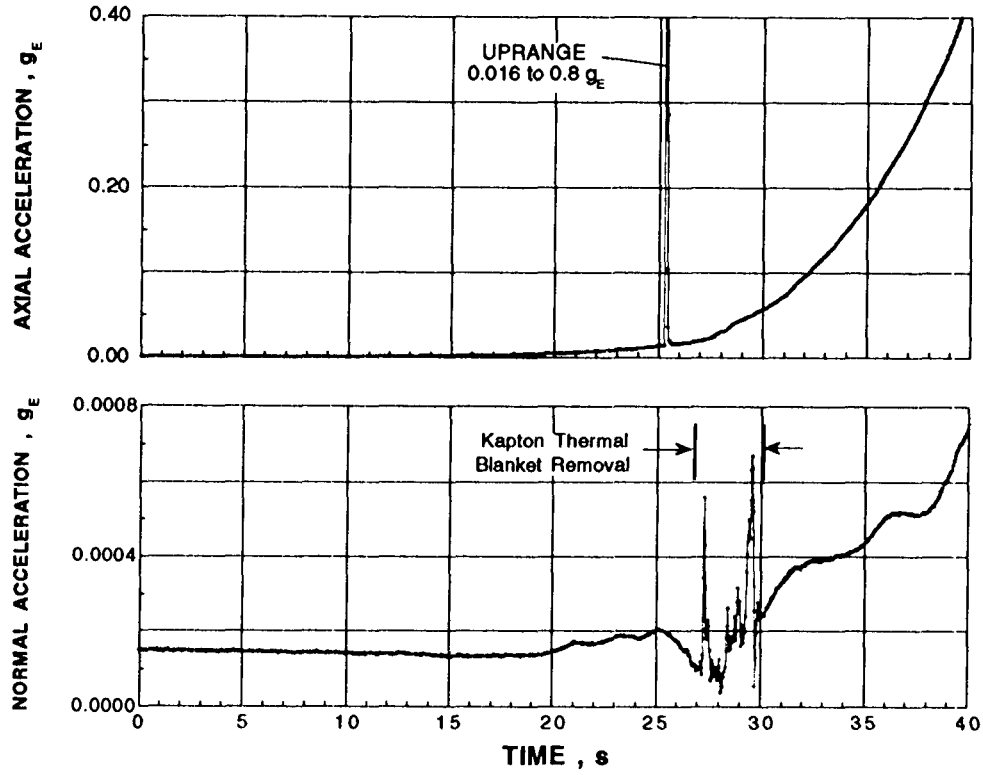


Figure 4. Axial and Normal Acceleration Measurements During Entry
( $0 \leq$ TIME $\leq 40$ s )

Figure 5 presents a continuation of the accelerometer data from 40 to 180 s. The axial accelerometer range changes to its maximum value of 40 g (full scale) at about 44 s. A short time later, both the Y-axis and X-axis accelerometers are separately automatically upranged to their next range level (0.8 g). The axial accelerometer show the key events of: (1) maximum dynamic pressure which closely corresponds to the maximum acceleration of 16.1 g, (2) firing of the pyrotechnic devise which jettisons the parachute canister (labeled "mortar fire"), and (3) the 6.2 g shock induced when the chute opens. The time of the maximum heating rate is included for completeness and it was calculated (along with the dynamic pressure) using the trajectory and atmosphere reconstruction results discussed in the subsequent section. As discussed in the following section, the normal acceleration data clearly show the two static instability regions predicted prior to flight using CFD techniques.[6]

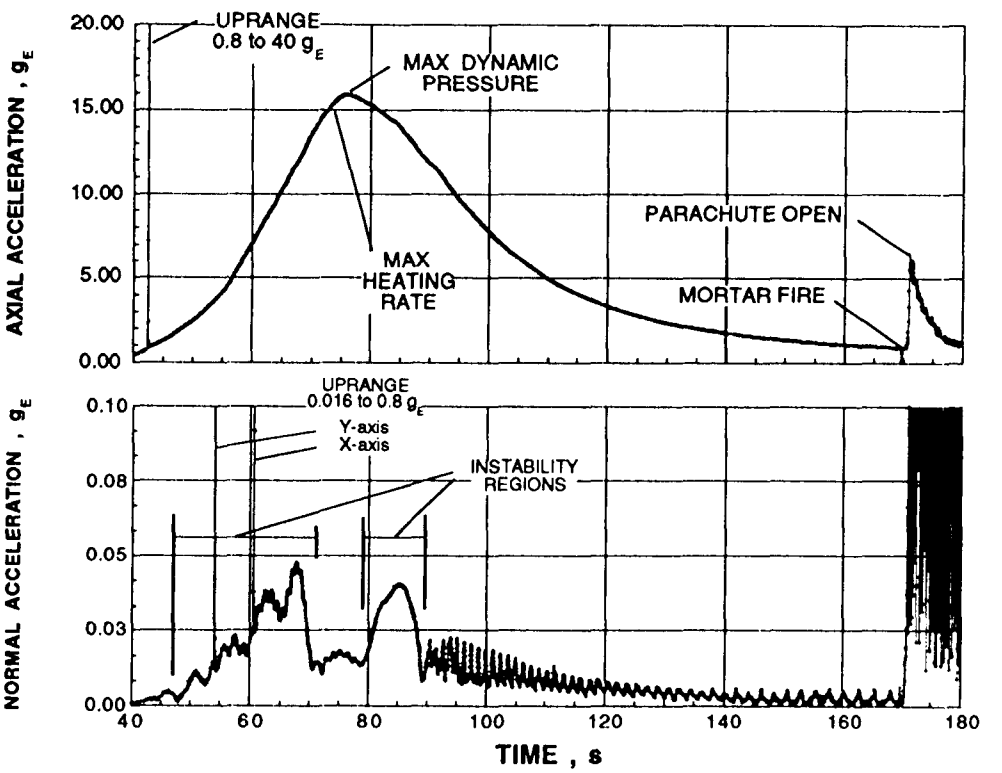


Figure 5. Axial and Normal Acceleration Measurements During Entry
( $40 \leq$ TIME $\leq 180$ s )

Figure 6 shows a continuation of this data during the parachute phase of the mission for a time period covering 180 s to 280 s from the atmospheric interface. The axial accelerometer shows the automatic down range to its next lowest scale of 0.8 g. Also seen are the separation of the heatshield and the separation of the lander onto a 20 m bridle as discussed earlier. At this time, there is a corresponding shift in the normal accelerations. This is accountable since the spacecraft center of gravity has shifted significantly, providing an additional small but spurious centripetal input into the accelerometers (which are not located exactly at the center of gravity).

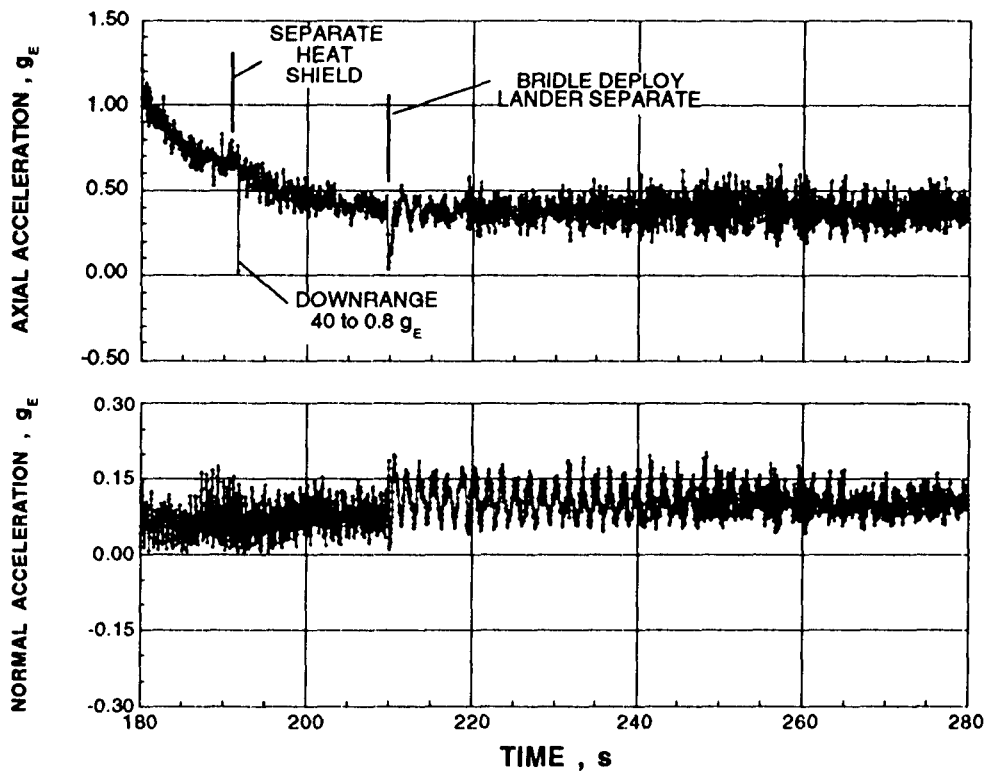


Figure 6. Axial and Normal Acceleration Measurements During Entry
( 180 $\leq$ TIME $\leq$ 280 s )

The next figure in this sequence, Figure 7, shows the remaining portion of the parachute phase down to airbag impact, including the first bounce on the surface of the planet, 280 s to 310 s past the atmospheric entry interface.

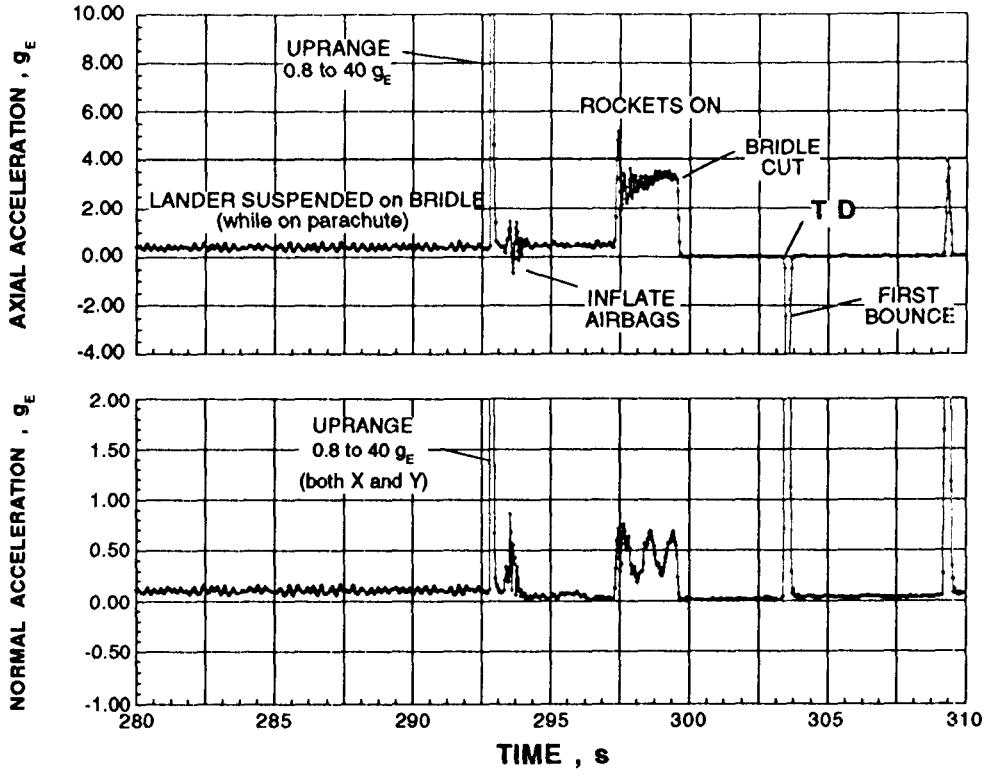


Figure 7. Axial and Normal Acceleration Measurements During Entry
( $280 \leq$ TIME $\leq 310$ s )

Both the axial and normal accelerometers are forced to go to full scale (40 g) in anticipation of landing. The uprange signature of the instrument is clearly seen in the figure. Shortly thereafter, the airbags are inflated, and then the RAD system is ignited. Note that a small component of the thrust appears in the normal direction. While the rockets are providing the retarding force, the bridle, from which the lander is suspended, is cut and the lander free-falls to the surface and begins to bounce. The first bounce spike due to impact with the surface is indicated in Figure 7. Figure 8 shows the data set collected while the lander bounced on the surface.

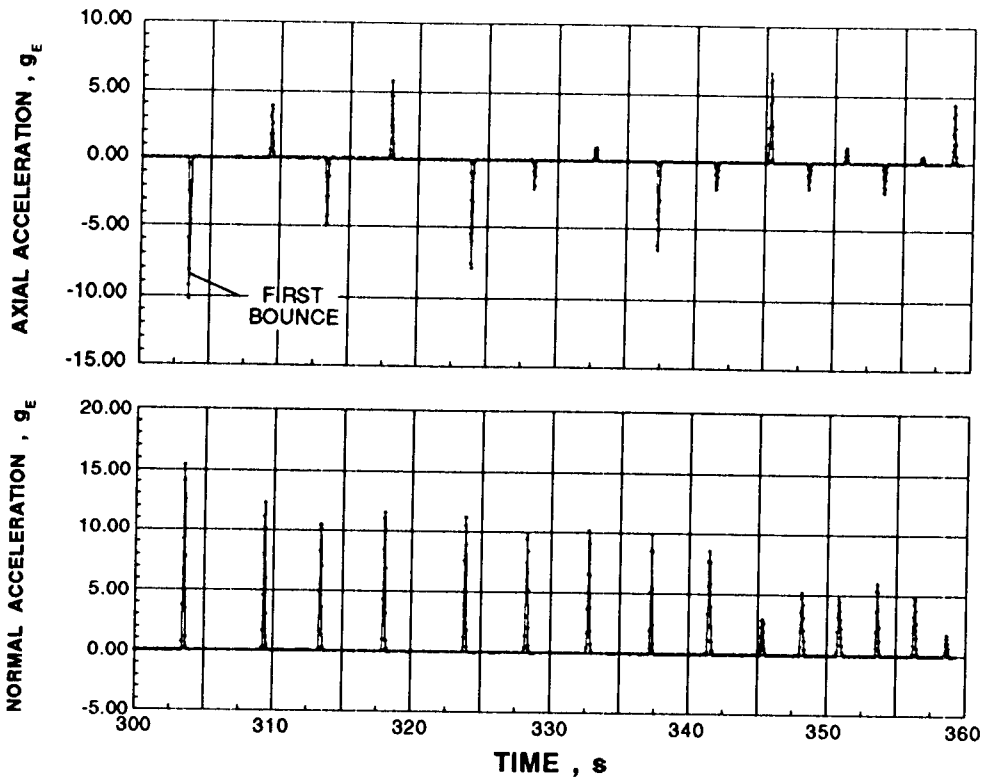


Figure 8. Axial and Normal Acceleration Measurements Following Impact
( $300 \leq$ TIME $\leq 360$ s )

Figure 8 slightly overlaps with Figure 7, so that all the acceleration data associated with the payload bounces can be viewed. As seen, 15 acceleration spikes were recorded, corresponding to 15 bounces. The spikes in the acceleration are the impulses imparted to the spacecraft as it contacted the surface. As the probe rose, the acceleration dropped to near zero, and remained near zero as the probe then fell to again contact the surface, which induced another acceleration spike. The telemetry was prematurely stopped at about 359.3 s, but the payload continued to bounce numerous times before coming to rest. A summary of the major entry, descent, and landing events is presented in Table 2.

Table 2. Pathfinder EDL Events Time-Ordered Listing

| Event | Time from Entry, s |
|---|---|
| Entry Interface ( Radius=3522.2 km) | 0 |
| Thermal Blanket Removal (begin) | 27.2 |
| Max Heat Rate | 73.2 |
| Max Dynamic Pressure | 76.1 |
| Mortar Fire | 169.6 |
| Parachute Open | 170.9 |
| Heatshield Separation | 190.3 |
| Bridle Deploy (Lander Sep.) | 209.6 |
| Inflate Airbags (begin) | 293.3 |
| Rocket Ignition | 297.3 |
| Bridle Cut | 299.5 |
| Touchdown (1st Bounce) | 303.4 |
| Last Recorded Bounce | 258.4 |
| Last Data Record | 359.3 |

## Landed Position Fix

Two independant methods were used to locate the actual landing site. The first method utilized landmark identification. Horizon features such as hills, knobs and craters are seen in the panoramic images from the lander. These features were easily identified and located on images of the surface obtained from the Viking orbiters, from which a very accurate (100 m) estimate of the lander's location was obtained. The second method utilized radiometric tracking from the lander in a manner not unlike the orbit determination task during cruise[7]. Table 3 gives the results of these two methods. The difference between the two positions is attributed to map-tie errors between the assumed location of surface features on current USGS maps and their actual positions relative to the Mars latitude/longitude grid. The position determined using radiometric tracking is assumed to be correct for trajectory reconstruction purposes.

Table 3. Landing Site Solutions

| Method | E. Longitude (deg) | Aerographic Latitude (deg) |
|---|---|---|
| Landmark Recognition | 326.45 | 19.33 |
| Lander Radiometric Tracking | 326.48 | 19.28 |

It is of interest to note that the final pre-flight footprint prediction contained the actual landing site. In fact, the center of this $3\sigma$ footprint prediction was within 0.5 km in downtrack and 5 km in crosstrack from the radiometric tracking estimate.[1,2,4]

## Flight Path

The Pathfinder post-flight entry trajectory has been reconstructed from on-board measurements taken during the vehicle's flight through the Mars atmosphere. For description simplicity, the trajectory is separated into two phases: (1) from the entry interface to the parachute deployment event (at approximately 170.9 s), and (2) the parachute descent, surface impact, airbag bounce, and roll/stop. Figure 9 shows the reconstructed in-plane trajectory parameters of altitude (as measured above the Mars reference ellipsoid), atmosphere relative velocity, and flight path angle.

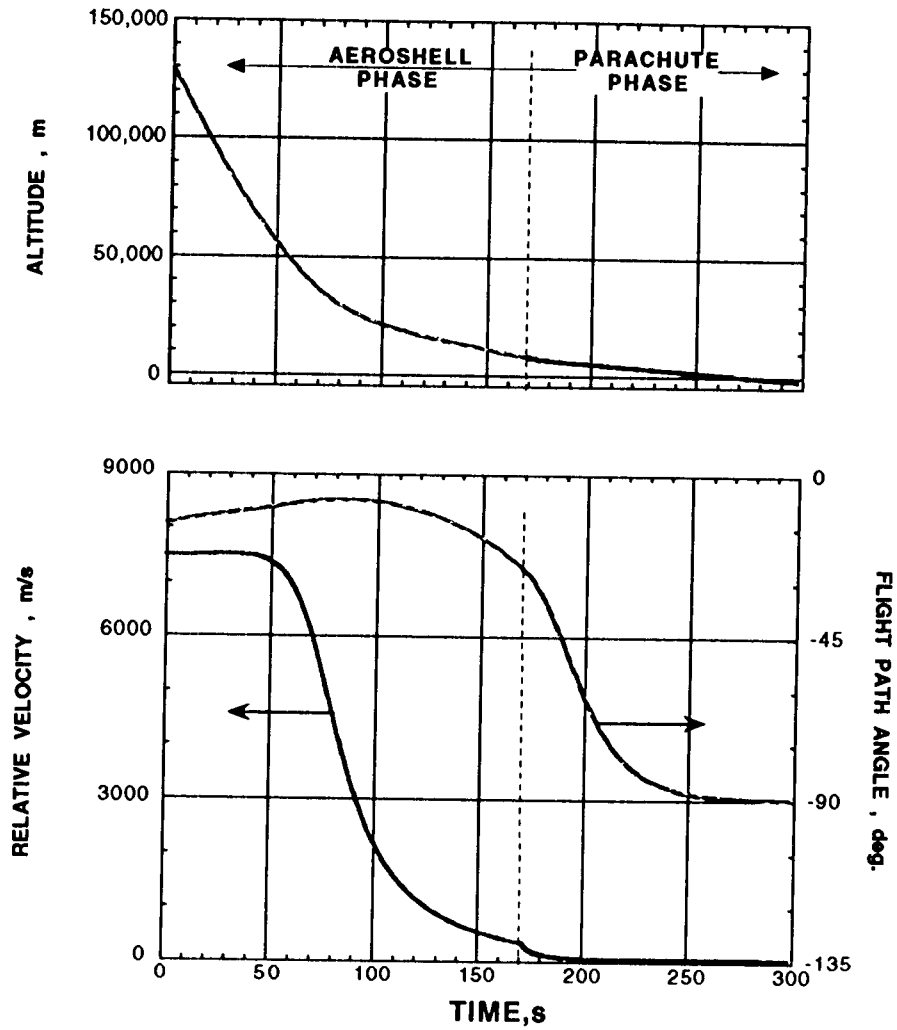


Figure 9. Pathfinder Reconstructed In-Plane Trajectory Parameters.

The reference time (t = 0) is at the entry interface altitude of about 130 km (a radius of 3522.2 km). The time interval labeled "Aeroshell Phase" on Figure 9 includes the free-molecule and transitional flow regimes, hypersonic, and supersonic continuum speed regimes of the aeroshell vehicle. The time interval which is labeled "Parachute Phase" includes the transonic through subsonic speeds while the payload is suspended from the parachute.

## Flight Path Reconstruction Via Statistical Estimation

An important objective of the overall reconstruction effort is to assess the accuracy of pre-flight computational models used for verification and validation of the EDL system during its development. To support this effort, a method for a-posteriori flight path estimation was developed that uses sensor data only and requires no a-priori dynamical modeling information. This approach, which blends accelerometer, altimeter, and ground-based measurements of received frequency using sequential filtering and smoothing techniques, yields a reconstruction of the trajectory that is largely free of influence from the dynamical models and modeling assumptions used in pre-flight design, analysis, and simulation work (e.g., vehicle aerodynamics). The resulting reconstruction products provide a basis for comparison with and evaluation of other reconstructions obtained from dynamical simulations.

The overall computational flow process is an adaptation of the aided-inertial navigation concept widely used in both terrestrial and space-borne navigation systems, in which external measurements are used to estimate corrections to position, velocity and attitude parameters computed from accelerometers and gyroscopes situated on the carrier vehicle[8,9]. The salient aspects of the adaptations made for use with Mars Pathfinder are discussed in more detailed below.

The first step in developing a reconstruction is the calculation of an initial estimate of the position and velocity history. This is accomplished by integration of the kinematic equations governing the flight path in a nonrotating, Mars-centered coordinate frame using accelerometer data and a model for the gravitational field of Mars. The initial conditions employed are the best estimate of the spacecraft state at the predicted time of entry interface computed by the ground-based navigation system. Unlike a conventional inertial navigation system, the spacecraft was not equipped with gyroscopes, therefore no direction calculation of the vehicle's attitude was possible. Since the spacecraft was designed to yield a nominally ballistic flight path (i.e., all aerodynamic or other contact forces experienced by the lander are parallel to its surface-relative velocity vector), the assumption of ballistic motion was employed in computing this initial reference trajectory.

Next, a linearized formulation of the discrete Kalman filter algorithm[10] is used to reduce measurements of received frequency and altitude sequentially, computing estimates of the deviation of the actual trajectory from the initial flight path estimate calculated via accelerometer data (designated the reference trajectory). The sequential filter program produces two different estimates of the corrected flight path, along with computations of the error covariance matrix associated with each estimate: the first is obtained by processing the received frequency and altimeter data from the initial time (predicted time of entry

interface) to the time of the lander's initial impact on the Martian surface; the second is obtained by processing the same data set, but with time running backwards, beginning with the time of impact and ending at entry interface. In addition to estimates of the deviations in position and velocity from the reference trajectory, the filter algorithm also computes estimates of the deflection of the contact force vector from the surface-relative velocity vector, and several additional parameters representing errors in the measurments, including accelerometer sensing errors, altimeter errors, and deviations of the carrier frequency transmitted by the spacecraft from the profile predicted prior to entry. The estimation of contact force deflection angles is analogous to the estimation of errors in attitude parameters computed from gyroscope outputs in a conventional aided-inertial navigation scheme.

The final step in the reconstruction process is to compute revised estimates of the position and velocity deviations from the reference trajectory, along with the deflection angle parameters and sensor error parameters, by combining the estimates derived from the forward and backward filtering of the received frequency and altimeter data. This reconciliation of the forward and backward estimates is accomplished using the Fraser-Potter smoothing algorithm[11], which statistically blends the two different estimates to obtain, ideally, minimum-variance estimates for all parameters incorporating all of the information gleaned from the complete data set.

An initial smoothed solution for the flight path is illustrated in Figures 10 and 11 below. Figure 10 presents time histories of the altitude, descent rate (altitude rate of change), and downrange rate (normal to the position vector and lying in the plane of the trajectory) during the entry phase up until parachute deployment occurred, approximately 170 s after entry interface. Figure 11 provides time histories of the same parameters for the terminal descent phase, from parachute deployment until the time at which the initial airbag impact on the surface occurred, approximately 305 s after entry interface. For comparison purposes, the accelerometer-computed reference trajectory and its associated error bars ($\pm 1\sigma$) are also shown. Note that the error bars in Figure 10 are indiscernible due to their small size. In addition, the error bars associated with the smoothed estimates are not shown due to their small size as well.

It is clear from Figure 10 that the reference trajectory computed from accelerometer data is an accurate representation of the flight path; the trajectory determined by the smoother is virtually indistinguishable. Figure 11 illustrates that the ballistic assumption employed in computing the reference trajectory is not as valid during the terminal descent phase as during entry, a result that was anticipated, due to likely oscillation of the parachute during this period. In particular, the descent rate of the lander during roughly the final 20 seconds of flight is seen to increase noticeably. The cause of this behavior is not understood at this time, and is still the subject of an ongoing evaluation effort. Also of note is the increase in the downrange rate that occurred during the retrorocket burn (between about 298 and 301.5 s after entry interface), leading to a horizontal velocity component of approximately 6 m/s at impact. This is attributed to a deflection of the net retrorocket thrust vector from the vertical of about 3 deg during the retro-burn, due to parachute oscillation prior to ignition. The descent rate at impact was approximately 10 m/s, close to the expected value. Both the horizontal and vertical components of impact velocity were well within the design envelope of the airbag landing system, which successfully brought the lander to rest approximately two minutes after the initial impact.

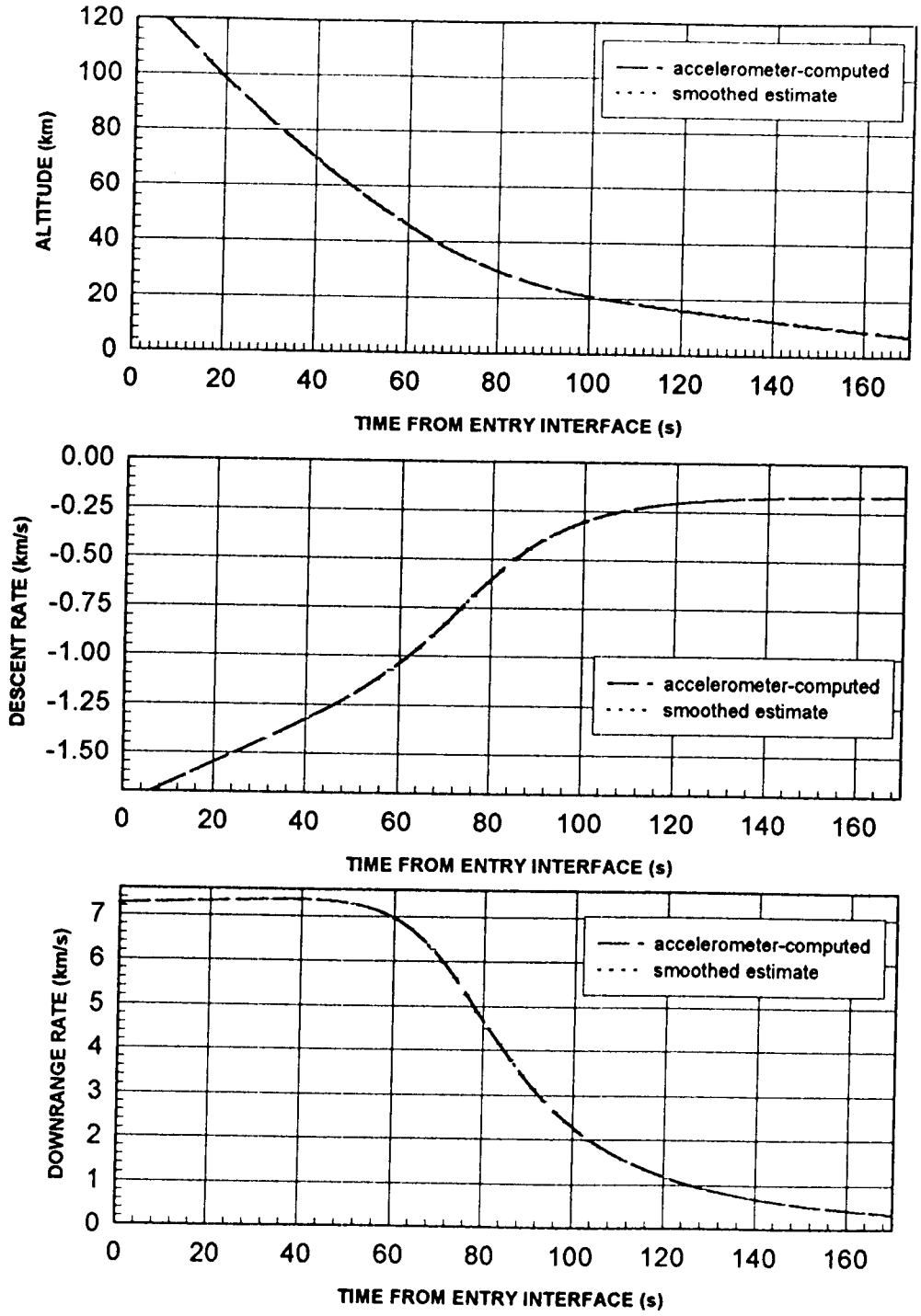


Figure 10. Smoothed Entry Reconstruction Results

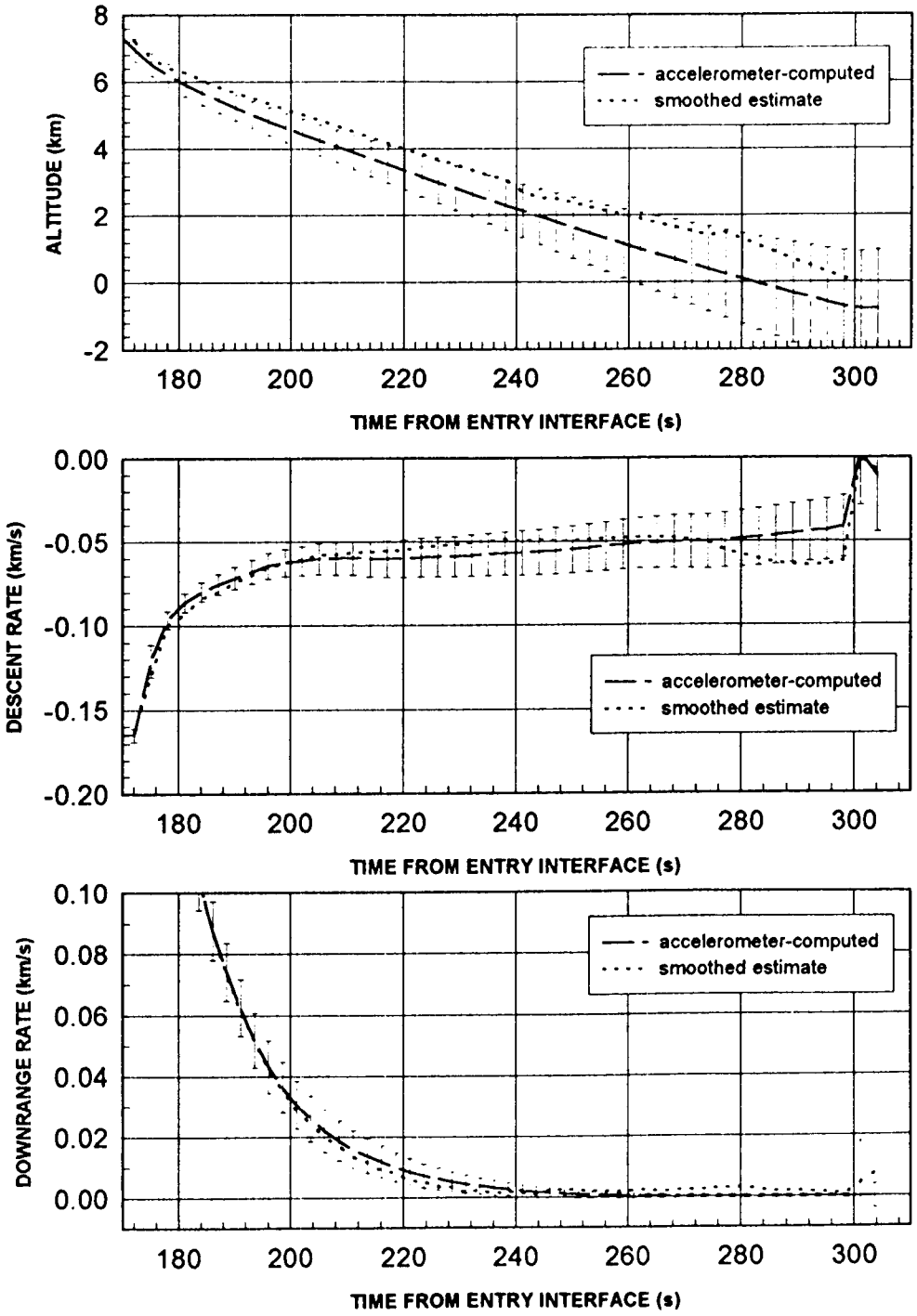


Figure 11. Smoothed Terminal Descent Reconstruction Results

## Roll Rate

During interplanetary cruise, the Pathfinder spacecraft was rotating about its principal axis at a 2 rpm roll rate. This roll rate was to remain unchanged through cruise-stage separation and into the atmospheric flight to provide a means of stability as the dynamic pressure decreased prior to parachute deployment and to null out any lift forces during the atmospheric entry. Expanding the scale of the data shown in Figure 4 but including data taken prior to encountering the atmospheric interface, Figure 12 shows an oscillation with a period of approximately 110 sec in the high-altitude accelerometer data.

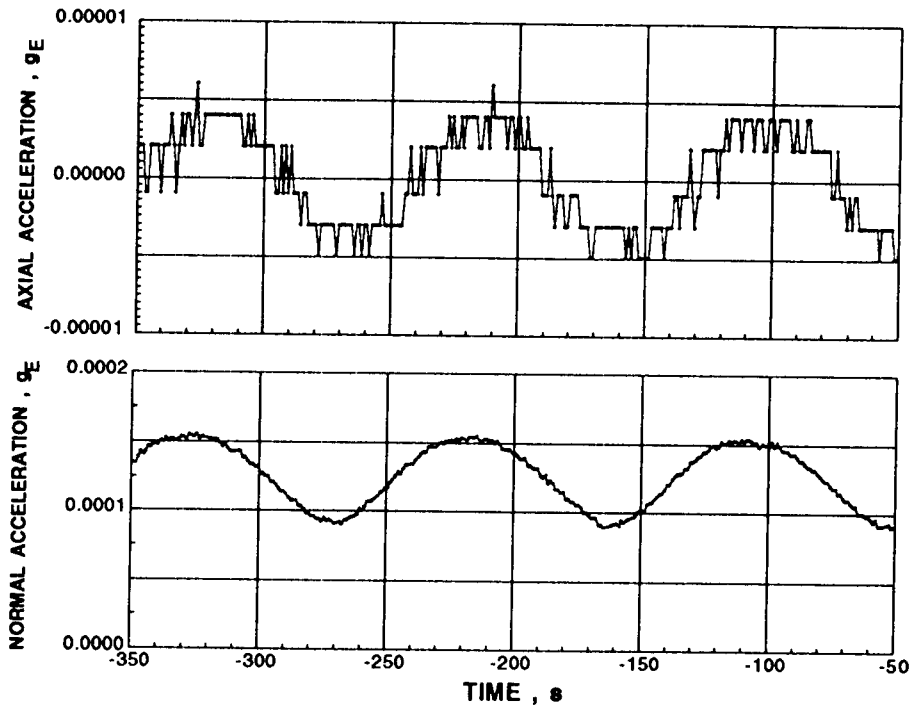


Figure 12. Axial and Normal Acceleration Measurements Prior to Atmospheric Entry ( $-350 \leq$ TIME $\leq -50$ s).

This motion in which the vehicle is coning about its principal axis is a result of the misalignment between the vehicle's body axes (defined by the aeroshell axis of symmetry) and the principal axes (defined by the aeroshell mass distribution). The vehicle roll rate can be derived from this motion as,

$$\omega_{obs} = \| ( 1 - I_{zz}/I_{xx}) \| \omega_z \tag{2}$$

Substituting the Pathfinder entry vehicle moment-of-inertia ratio of 1.27273 and the observed 0.0090909 Hz frequency of Figure 12 yields, a 1.99999 rpm roll rate. Hence, cruise-stage separation did not significantly alter the entry vehicle spin. While roll-rate data within the atmosphere was not obtained, a means for significant roll damping does not exist (no fluid slosh, a low degree of inertial coupling, and minor boundary layer aerodynamic effects). Hence, this 2 rpm roll rate was likely maintained throughout the atmospheric entry.

**Angle-of-Attack Profile**

Based on the spacecraft accelerometer measurements, it is clear that the Pathfinder spacecraft did not follow a purely ballistic entry flight-path. Several regions of non-zero normal acceleration are shown in flight data presented in Figures 5 and 6. In each of these regions, the resultant force vector was not parallel to the relative velocity vector; hence, the vehicle was at a non-zero total angle-of-attack. Here, total angle-of-attack is defined as the angle between the vehicle's axis of symmetry and the relative velocity vector.

Total angle-of-attack during the aeroshell entry phase can been estimated in one of several ways with use of the spacecraft accelerometer measurements and the preflight aerodynamics database.

$$A_n = (\rho V^2 C_n S)/(2m) \tag{3}$$

$$A_n/A_z = C_n/C_A \tag{4}$$

The normal-force coefficient, $C_n$, in eq. (3) and the aerodynamic coefficient ratio $C_n/C_A$ in eq. (4) are each functions of total angle-of-attack and relative velocity. Hence, total angle-of-attack could be estimated with either of these relations. In this analysis, total angle-of-attack was estimated with use of eq. (4) as no reliance on an atmospheric density prediction was required and the continuum hypersonic $C_A$ uncertainty for a 70 deg sphere-cone at small angles-of-attack is low.[12,13] With use of the relative velocity profile from the best estimated trajectory presented in Figure 9 and the accelerometer data as shown in Figure 13a, the preflight aerodynamic database[12] was interpolated to produce an estimate of total angle-of-attack. This total angle-of-attack estimate is presented in Figure 13b.

Note that a total angle-of-attack estimate is not obtainable in this manner for the first 20 sec of the atmospheric entry. However, as the density increases above 1.0e-07 kg/m$^3$ at an altitude of approximately 95 km, the $A_n/A_z$ signal is strong enough to discern vehicle attitude. Further detail on the rarefied portion of the Pathfinder atmospheric entry is provided in Reference 5.

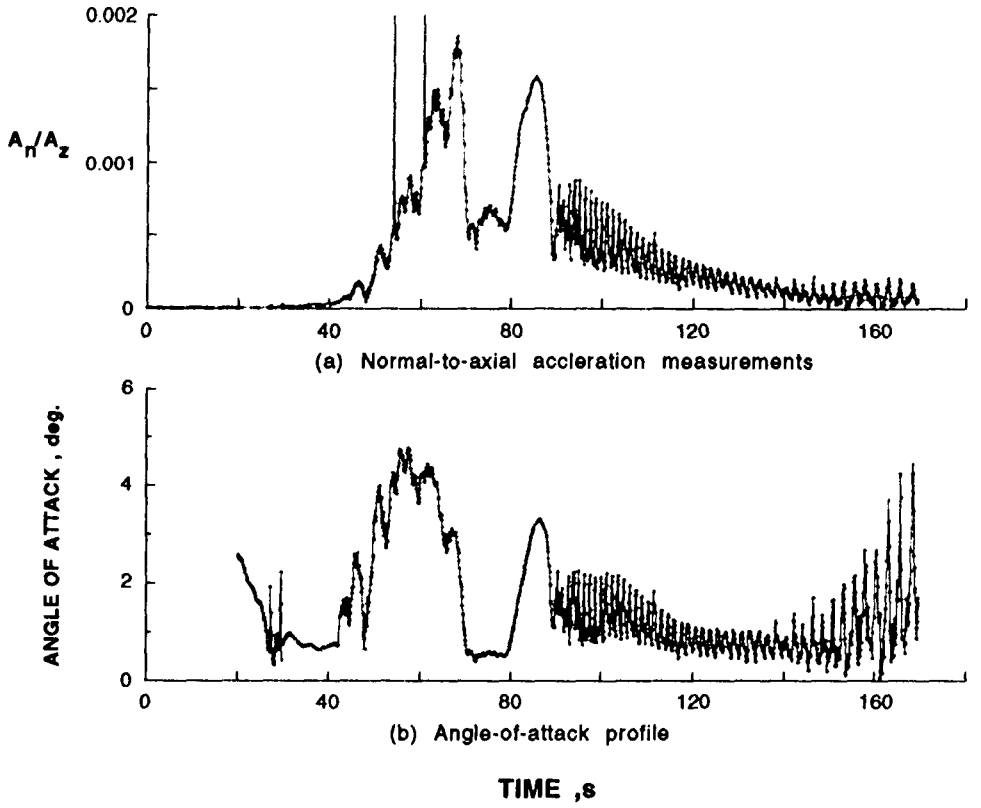


Figure 13. Normal-to-axial acceleration measurements and total angle-of-attack estimate during aeroshell phase.

The presence of two hypersonic static instability regions and a supersonic dynamic instability region as predicted in Refs. 6, 12, and 13 is clearly evident in Figure 13b. In fact, the hypersonic static instability regions (centered at approximately 55 and 85 sec) are strong enough to be evident in both Figure 13b (the angle-of-attack estimate derived with the preflight aerodynamic database) and Figure 13a (the straight accelerometer data). This derived angle-of-attack estimate bears striking similarity to the pre-flight prediction presented in Reference 14. At the time of peak heating, the vehicle was at a total angle-of-attack of approximately 3 degrees.

**Parachute Deployment Algorithm Performance**

Both a primary and backup system were developed to initiate deployment of the parachute. The objective of these in-flight software process was to deploy the parachute as close to a dynamic pressure of 600 $N/m^2$ as possible. Without an inertial measurement unit

or gyroscopes, the primary parachute deployment algorithm relied solely on accelerometer readings and consultation of a pre-determined set of entry deceleration profiles, stored in curve-fit form.[15,16] This algorithm was initiated at cruise-stage separation and was responsible for interpreting the deceleration pulse, scheduling the appropriate time to initiate parachute deployment, and firing the parachute mortar. If the flight software determined that accelerometer readings were invalid, the backup parachute deployment system would be enabled. This system initiates deployment of the parachute at a fixed time, stored as a flight software parameter.[17]

To minimize risk, parameter updates to the primary and secondary parachute deployment systems were designed into the operations navigation procedures.[2] Software parameters which determined the primary system's curve-fit, fault-protection logic, and deceleration sampling strategy as well as the fixed-time backup could be updated during flight (prior to entry). Update criteria and command approval strategies were also established and simulated in several operations readiness tests. Parameter updates were expected as the spacecraft's entry state and predicted atmosphere varied. The final flight software parameter update was relayed to the Pathfinder spacecraft at approximately 11:00 pm PDT on 7/2/97.[2]

Analysis of the accelerometer measurements conclusively demonstrates that the parachute was deployed based on the primary algorithm. Based on the deceleration history provide in Figure 5, Reference 2 demonstrates that the primary parachute deployment algorithm should have fired at 170 sec past the atmospheric interface. In contrast, the fixed-time backup parameter would have deployed the parachute at 163 sec. Based on the trajectory reconstruction analysis presented in this paper, the parachute deployment altitude was approximately 7.9 km above the Mars reference ellipsoid (9.5 km above the surface) at a dynamic pressure of approximately 583 $N/m^2$ and a Mach number of 1.7. This is extremely close to the parachute deployment design target (600 $N/m^2$), hence, the primary parachute deployment algorithm is deemed to have performed well.

It is interesting to note the algorithm's possible performance had there been no flight software parameter update process. As shown in Figure 14, without the 7/2/97 software parameter update, the original fixed-time backup parachute deployment time would have resulted in a deployed parachute 16 sec early at a dynamic pressure close to 850 $N/m^2$ (well above the design limit of 703 $N/m^2$). However, as discussed in Reference 2, after modification during the 7/2/97 parameter update process, the backup fixed-time deployment would have occurred 7 sec early at a dynamic pressure of approximately 695 $N/m^2$. This demonstrates that the parameter update process performed by the operations navigation team in the final days of interplanetary cruise increased the probability of mission success.

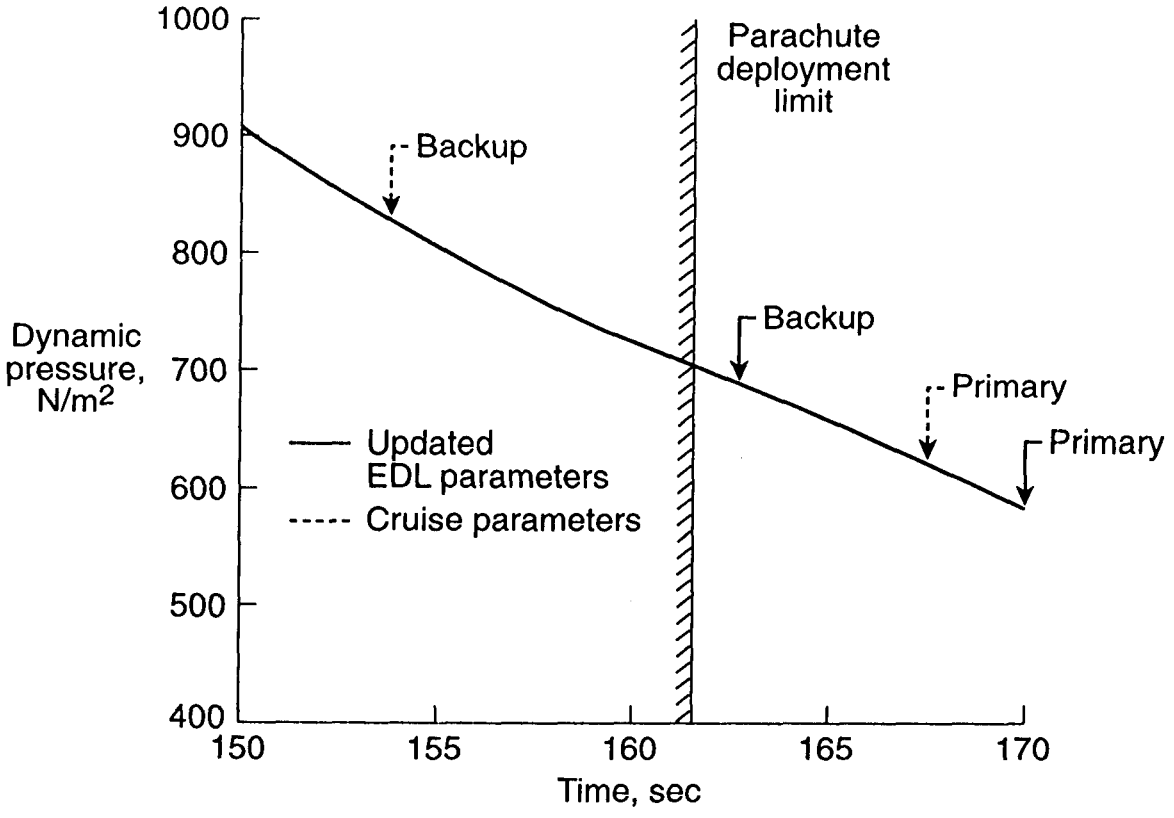


Figure 14. Mars Pathfinder Parachute Deployment Algorithm Performance.

## TERMINAL DESCENT DYNAMICS

As shown in Figures 15 and 16, a three dimensional multibody dynamic model was developed using the ADAMS program[18,19]. This model was intended to simulate the dynamic behavior of the system over the entire terminal descent phase, from parachute deployment until surface impact. As a simulation effort for the EDL reconstruction, the dynamic model described above is utilized to determine the dynamic configuration of the multibody system (parachute/backshell/lander), to characterize the drag performance of the parachute, and to estimate the wind effect during the terminal descent. This section summarizes the engineering reconstruction effort for the Mars Pathfinder terminal descent dynamics.

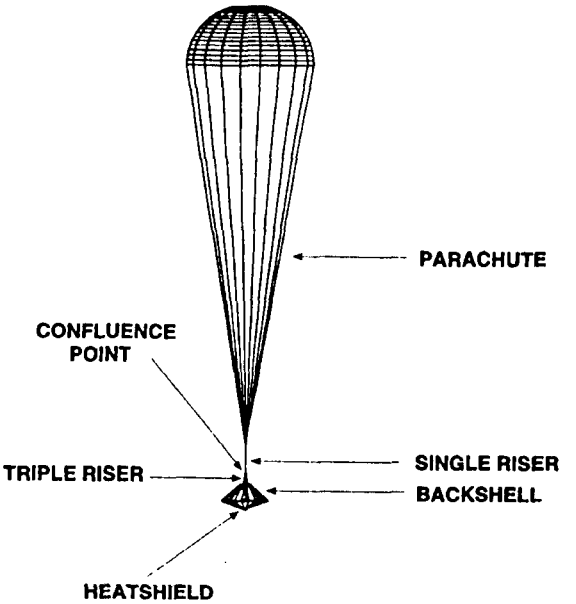


Figure 15. EDL Model at Start of Simulation

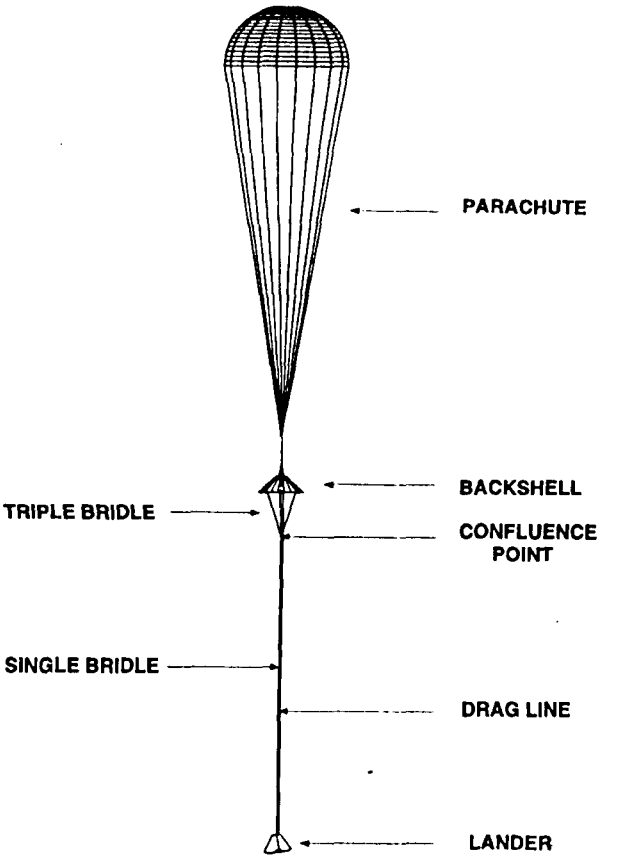


Figure 16. EDL Model During Final Descent

Figure 17 shows the time histories and Fourier amplitude plots of the accelerations measured by the on-board science accelerometers from parachute deployment to airbag inflation. The corresponding time histories and Fourier amplitude plots of the accelerations from the EDL reconstruction simulation are illustrated in Figure 18. Excellent agreement in frequency response is observed between the Fourier amplitude plots of Figures 17 and 18, except in the Z-acceleration. In the EDL model, the stiffness values of the parachute risers and the lander bridles are artificially reduced to improve the numerical convergence and to reduce simulation time. As a result, the EDL model is more flexible than the flight system along the Z-axis. However, this is not critical for predicting the performance of the EDL system during terminal descent.

In general, a good comparison in time history response is also observed between the actual flight accelerometer data and the simulated accelerations, particularly after the lander separation, which occurred at approximately 39 s after parachute deployment. Shortly after parachute deployment, it is seen that the simulated accelerations are different from the flight data and damp out much faster. The difference observed could be minimized by better modeling the parachute opening dynamics and by reducing the damping in the model. The "beat" phenomenon in the simulated accelerations is due to a 2 rpm spin

imposed on the system. Since the beat phenomenon is much less in the real flight data, the spin rate of the flight system must have been very small during terminal descent.

To characterize the drag performance of the parachute from the flight data, an extensive effort has been conducted to identify the drag coefficient of the parachute by minimizing the difference between the simulated flight trajectory profiles and those estimated from the flight accelerometer and Doppler data.

By adjusting the drag coefficient of the parachute, a good match can be achieved between the simulated trajectory profiles (altitude, flight path angle and descent velocity vs. time) and those estimated from the flight data, as illustrated in Figure 19. It is interesting to note that there is no effect of wind included in the results shown in Figure 19. This indicates that winds were calm during Pathfinder's terminal descent.

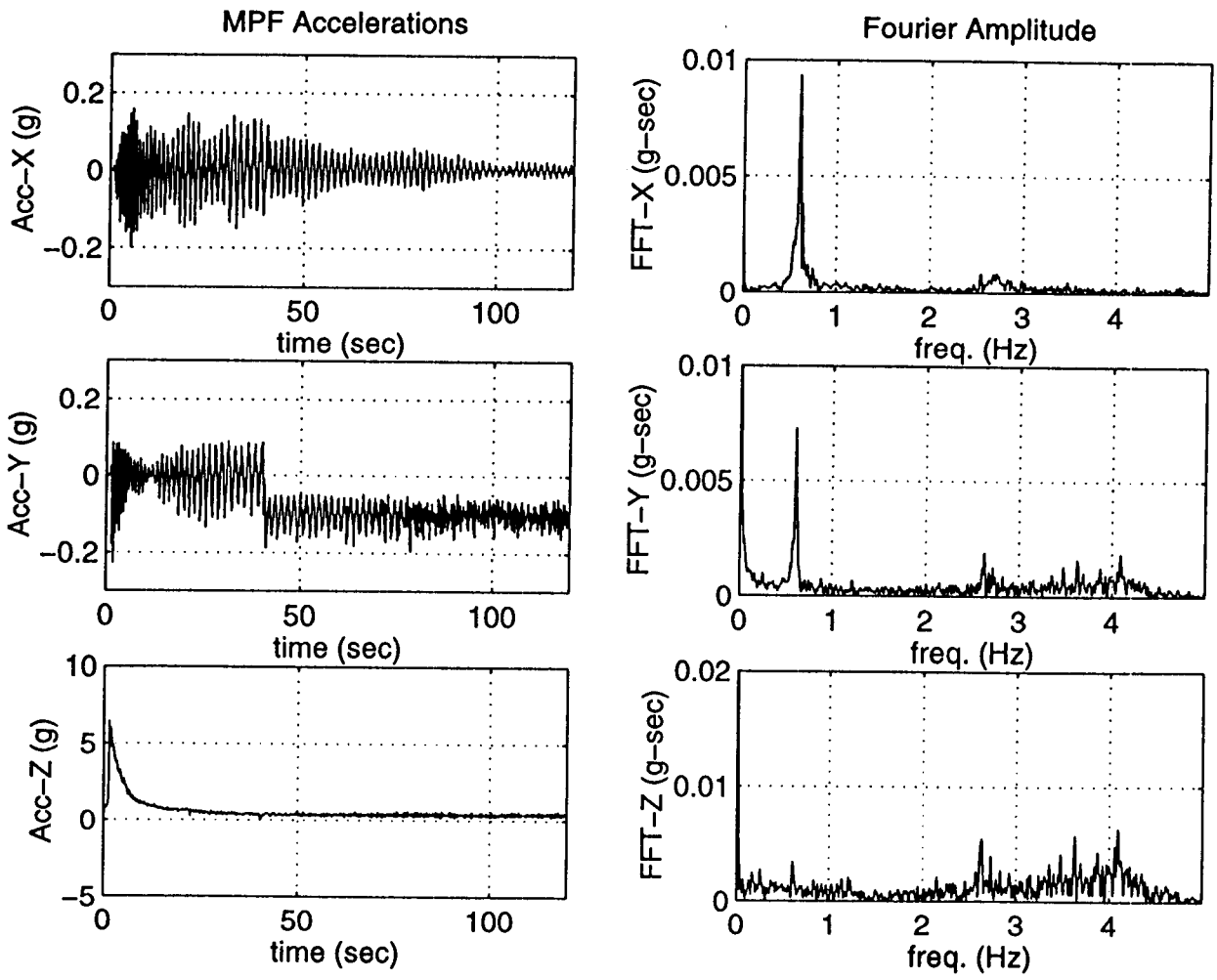


Figure 17. Flight Accelerations during Terminal Descent

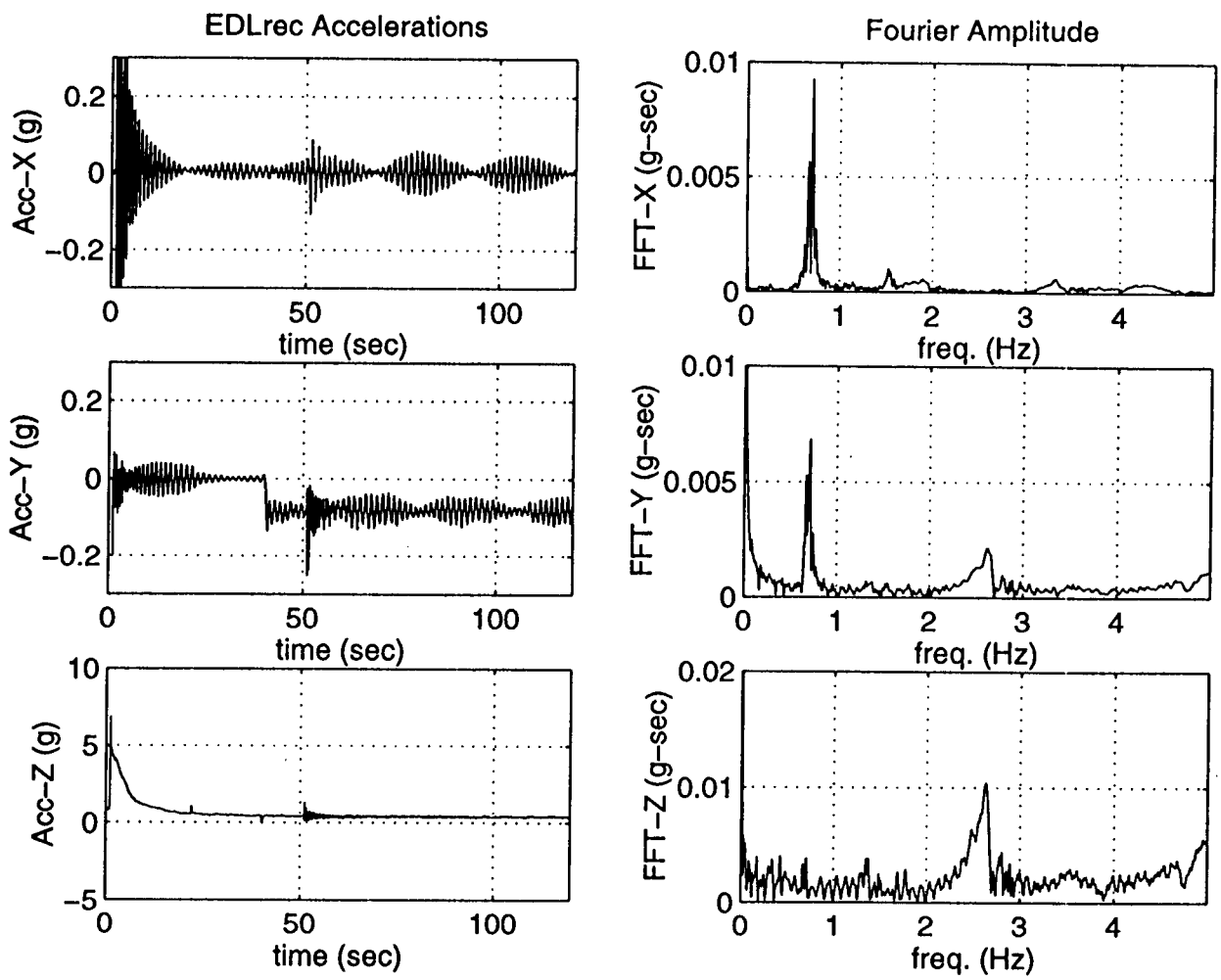


Figure 18. Simulated Accelerations from Terminal Descent Reconstruction

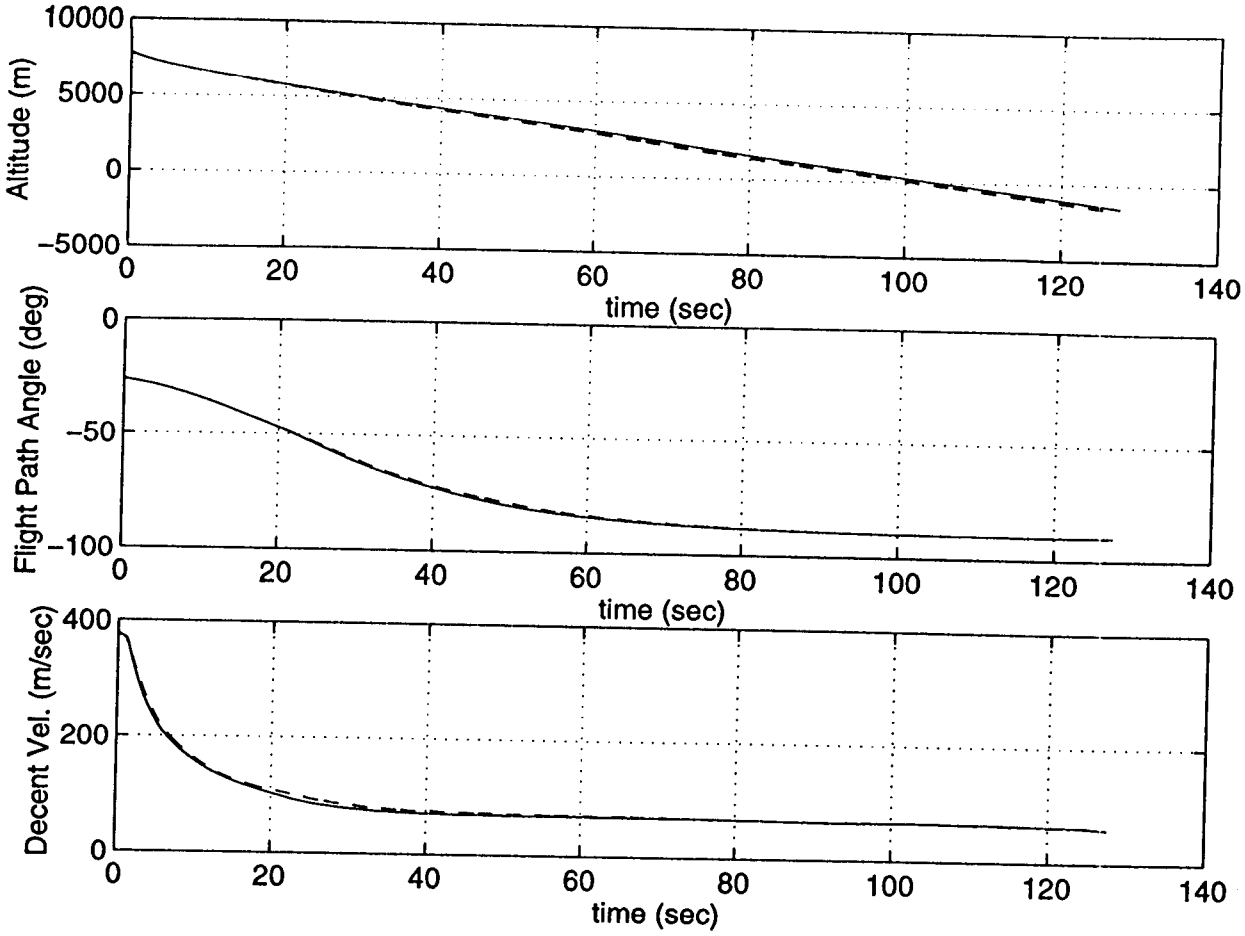


Figure 19. Comparison of Trajectory Profiles without Wind Disturbance (solid line: flight estimate, dashed line: simulation)

## MARS ATMOSPHERE PROFILE

An engineering profile of the Mars atmosphere during the Pathfinder entry, in terms of temperature, pressure, and density, has been constructed. Figure 18 shows the derived Mars atmosphere atmosphere state properties (i.e. density, pressure, and temperature) during two phases of the descent, namely, before and after parachute deployment. The procedure for calculating the atmosphere properties are essentially the same for both phases. However, the parachute phase is singled out because there is typically more significant variations in the acceleration data due to motions on the parachute and smoothing of these results is required.

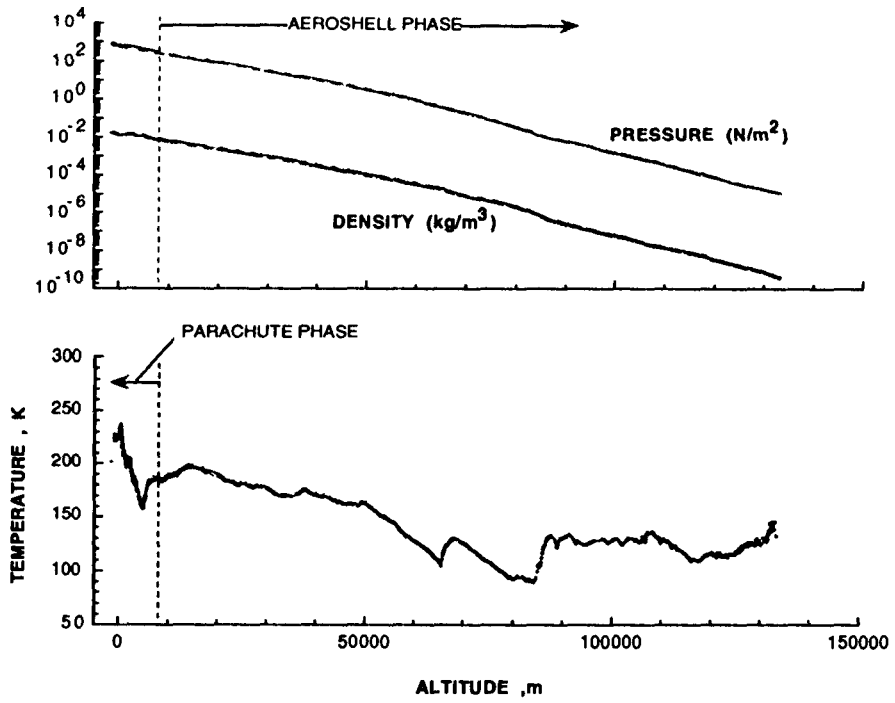


Figure 18. Computed Atmosphere State Properties During Pathfinder Descent

The atmosphere properties shown are calculated independent of the trajectory parameters. The top graph of Figure 15 shows the density extracted from the acceleration data using the Pathfinder aerodynamic database[12]. This figure is the result of a point-by-point transformation using,

$$\rho = \frac{2A_z}{V^2 C_A \left(\frac{S}{m}\right)} \tag{5}$$

where V is the relative velocity obtained from the trajectory reconstruction process discussed earlier, $A_z$ is the measured acceleration along the axial direction, $C_A$ is the axial aerodynamic coefficient, and (S/m) is the area to mass ratio of the probe. The values of $C_A$ are flight regime dependent, and since all flight regimes from free-molecule flow to subsonic flow are encountered during entry, an iterative scheme has been developed to obtain the proper value of this aerodynamic coefficient in the procedure. This involves calculating the classical scaling parameters such as Knudsen, Reynolds, and Mach numbers

using an apriori guess at density as a starting point. The density profile shown in Figure 15 is similar to the reconstructed profile from the Viking I Lander data.[20]

Once density is obtained, then it can be used to calculate pressure from the hydrostatic equation. That is,

$$\frac{dp}{dh} = -\rho g \tag{6}$$

where g is the gravitation acceleration at altitude, h. This equation is integrated from a starting value of pressure, $p_0$ which is adjusted to provide a smooth variation at large altitudes. Slight errors in $p_0$ produce large variations in temperature, since the density at these large altitudes is also a small quantity.

The remaining variable, temperature, is calculated from the equation of state. That is,

$$T = \left(\frac{M}{R}\right)\frac{p}{\rho} \tag{7}$$

where M is the mean molecular weight (43.2685 kg/kmol), and R is the Universal gas constant (8314.34 J/kmol-K). For the data shown in Figure 18, M is assumed to have a fixed value. This will produce a small error in the temperature calculations at very high altitudes, roughly above about 120 km. The temperature results are shown as the bottom graph in Figure 18. Also shown are the landed pressure and temperature measurements of 683 $N/m^2$ and 202 K. These values yield a surface density of 0.0176 $kg/m^3$.

## CONCLUSIONS

The Pathfinder entry trajectory and Mars atmosphere profile have been reconstructed from the flight data. The flight data indicate that the Pathfinder EDL system performance was within the expected ranges during all phases of the Mars atmospheric flight. Preflight estimates of aeroshell performance, aerodynamic stability, and landing location have been confirmed. Validation of the parachute deployment flight software algorithm design has also been performed. Furthermore, the terminal descent system, culminating in RAD system firing and airbag deployment, performed flawlessly. Estimation of the Mars atmosphere indicates that the atmospheric properties are similar to that observed by the Viking spacecraft in 1976.

## ACKNOWLEDGEMENTS

The work described in this paper was performed at the NASA Langley Research Center and at the Jet Propulsion Laboratory, under contract with the National Aeronautics and Space Administration.

## REFERENCES


1. Golombek, M.P., et al, "Overview of the Mars Pathfinder Mission and Assessment of Landing Site Predictions," *Science*, Vol. 278, 5 December 1997, pp. 1743-1748.

2. Braun, R.D., Spencer, D.A., Kallemeyn, P.H., and Vaughan, R.M., "Mars Pathfinder Amospheric Entry Navigation Operations," AIAA 97-3663, presented at the 1997 AIAA GNC, AFM, and MST Conference and Exhibit, New Orleans, Louisiana, August 11-13, 1997.

3. Wood, G.E., Asmar, S.W., and Rebold, T.A., "Mars Pathfinder Entry, Descent and Landing Communications," TDA Projress Report 42-131, Jet Propulsion Laboratory, 15 November 1997.

4. Vaughan, R.M., Kallemeyn, P.H., Spencer, D.A., and Braun, R.D., "Navigation Flight Operations for Mars Pathfinder," AAS 98-145, AAS/AIAA Space Flight Mechanics Meeting, Monterey, CA, February 9-11, 1998.

5. Moss, J. N., Blanchard, R. C., Wilmouth, R. G., and Braun, R. D., "Mars Pathfinder Rarefied Aerodynamics: Computations and Measurements," AIAA Paper 98-0298, 36th AIAA Aerospace Sciences Meeting, Reno, NV, January 12-15, 1998.

6. Gnoffo, P.A., Weilmuenster, K.J., Braun, R.D., and Cruz, C.I., "Influence of Sonic Line Location on Mars Pathfinder Probe Aerodynamics," *Journal of Spacecraft and Rockets*, Vol. 33, No. 2, March-April, 1996, pp. 169-177.

7. Folkner, W.M., Yoder, C.F., Yuan, D.N., Standish, E.M., and Preston, R.A., "Interior Structure and Seasonal Mass Redistribution of Mars from Radio Tracking of Mars Pathfinder," *Science*, Vol. 278, 5 December 1997, p. 1749.

8. Schmidt, S. F., "The Kalman Filter: Its Recognition and Development for Aerospace Applications," *Journal of Guidance and Control*, Vol. 4, No. 1, Jan.-Feb. 1981, pp. 4-7.

9. Brown, R. G., *Introduction to Random Signal Analysis and Kalman Filtering*, John Wiley & Sons, New York, 1983, pp. 222-229.

10. Gelb, A. (Ed.), *Applied Optimal Estimation*, M.I.T. Press, Cambridge, 1974, p. 189.

11. Fraser, D. C., and J. E. Potter, "The Optimum Linear Smoother as a Combination of Two Optimum Linear Filters," *IEEE Transactions on Automatic Control*, Vol. AC-14, No. 4, Aug. 1969, pp. 387-390.

12. Engelund,W.C., Gnoffo, P.A., Cruz, C.I., Braun, R.D., and Weilmuenster, K.J., "Aerodynamic Characteristics of the Mars Pathfinder Atmosphere Entry Configuration," NASA TM (in preparation).

13. Braun, R., Powell, R., Engelund, W., Gnoffo, P., Weilmuenster, K., and Mitcheltree, R., "Mars Pathfinder Six-Degree-of-Freedom Entry Analysis," *Journal of Spacecraft and Rockets*, Vol. 32, No. 6, Nov.-Dec., 1995, pp. 993-1000.

14. Spencer, D.A., and Braun, R.D, "Mars Pathfinder Atmospheric Entry: Trajectory Design and Dispersion Analysis," *Journal of Spacecraft and Rockets*, Vol. 33, No. 5, Sept.-Oct., 1996, pp. 670-676.

15. Singh, G., "Mars Pathfinder Accelerometer Algorithm," Jet Propulsion Laboratory, JPL IOM 3456-95-12, Mar. 1995.

16. Spencer, D., "Mars Pathfinder Parachute Deployment Accelerometer Algorithm Parameters," Jet Propulsion Laboratory, JPL IOM 312/96.2-004, May 1996.

17. Spencer, D., "Mars Pathfinder Fixed-Time Backup," Jet Propulsion Laboratory, JPL IOM 312/95.2-2059, April 1995.

18. Smith, K.S., Peng, C-Y., and Behboud, A., "Multibody Dynamic Simulation of Mars Pathfinder Entry, Descent and Landing," JPL Document D-13298, 1 April 1995, Jet Propulsion Laboratory, California Institute of Technology, Pasadena, California.

19. ADAMS/Solver Reference Manual, Version 8.0, 15 November 1994.

20. Blanchard, R.C., Wilmoth, R.G., and Moss, J.N., "Aerodynamic Flight Measurements and Rarefied Flow Simulations of Mars Entry Vehicles," *Journal of Spacecraft and Rockets*, Vol. 34, No. 5, Sept.-Oct., 1997, pp. 687-690.